# New Feedback Linearization-Based Control for Arm Trajectory Tracking of the Furuta Pendulum

Carlos Aguilar-Avelar and Javier Moreno-Valenzuela, *Member, IEEE*

***Abstract*—The purpose of this paper is to introduce a new trajectory tracking controller applied to the Furuta pendulum; where the arm tracks a desired time-varying trajectory, while the pendulum remains regulated at the upward position. This controller is derived from the input–output feedback linearization technique. The rigorous analysis of the internal dynamics is presented, showing that the tracking error and the regulation error trajectories are uniformly ultimately bounded. Experimental results show the validity of the introduced theory. Additionally, a detailed experimental study is also presented, where a PID controller and an output tracking controller are compared with respect to the new algorithm, which presents the best performance.**

***Index Terms*—Feedback linearization, Furuta pendulum, internal dynamics, real-time experiments, trajectory tracking.**

## I. Introduction

UNDERACTUATED mechanical systems have more degrees of freedom (DOF) than actuators to control [1]. Their uses are common in a lot of applications as robot mobile systems, vehicles used on space or under the sea (with special features that increase difficulties to control), or systems whose mathematical model includes joint flexibility for control. The rotary inverted pendulum, which is better known as Furuta pendulum in honor of its inventor [2], [3], is a well-known underactuated mechanical system that is extensively used by many control researchers to test linear and nonlinear techniques [4], [5]. This mechanism consists of an arm rotating in the horizontal plane and a pendulum rotating in the vertical plane. The system has only one actuator that provides torque input at the arm.

To control the behavior of this system, three classical control objectives can be found in the literature. First, starting from the natural rest position, the swing-up problem must be solved in order to take the pendulum from the downward to the upward position. After this, the stabilization problem must be addressed in order to regulate the pendulum at the upward unstable position. Finally, the trajectory tracking problem is introduced, such that the arm tracks a desired time-varying trajectory, while the pendulum remains regulated at the upward position. This paper is devoted to the trajectory tracking problem, introducing a new controller derived from input–output feedback linearization.

From the literature review, we have found that most of the work on control of underactuated mechanical systems, including the Furuta pendulum, is devoted to the regulation problem, e.g., [6]–[23]. Regarding the swing-up problem on the Furuta pendulum, model predictive control, energy-based algorithms, nonlinear control, sliding mode control, and fuzzy control techniques have been applied [24]–[29]. We have found that just a few works address the trajectory tracking problem in underactuated systems [30]–[38]. Furthermore, in particular for the Furuta pendulum, the trajectory tracking problem is rarely found in the literature [39]–[42], and deserves a special revision.

Feedback linearization is a control technique commonly used in nonlinear systems; see for example [43] and [44]. The basic idea of the feedback linearization control is to define a proper output function. By computing the time derivative of the output along the trajectories of the open-loop system, the controller is derived such that the resulting closed-loop system in terms of the output is linear and time-invariant. The whole closed-loop system in this methodology should be found using a coordinate transformation that leads to the so-called external and internal dynamics.

Previous works on the application feedback linearization technique for controlling underactuated mechanical systems are given below. A constructive methodology based on classical feedback linearization and Lyapunov design for 2-DOF underactuated mechanical systems was presented in [23]. This scheme only addresses the stabilization problem and the methodology to calculate the zero-dynamics disagrees with the theory introduced in [43] and [44]. In [22], an input-output feedback linearization controller was applied to a Furuta pendulum for the stabilization problem, where genetic algorithms were used for tuning the control parameters. Internal dynamics was assumed to be unstable (without proof), such that, an additional PD action was applied to stabilize the system. Numerical simulations showed the viability of the proposed algorithm. In [41], an output tracking nonlinear controller was presented for a frictionless model of the Furuta pendulum. Notwithstanding, the zero-dynamics was not obtained according to the theory available. Finally, in [35] an adaptive fuzzy controller based on a feedback linearizing scheme was presented for the trajectory tracking control of the inverted-pendulum on a cart system. No discussion on the zero-dynamics obtained with input–output feedback linearization framework was provided.

The contribution of this paper is twofold. The first consists in introducing a new trajectory tracking controller, which is based on the feedback linearization technique. Note that the controller

Manuscript received February 17, 2014; revised May 11, 2015 and August 3, 2015; accepted August 25, 2015. Date of publication October 1, 2015; date of current version February 24, 2016. Recommended by Technical Editor O. Kaynak. This work was supported in part by the CONACyT Project no. 176587, and SIP-IPN, Mexico.

The authors are with the Instituto Politécnico Nacional-CITEDI, Tijuana, B.C. 22510, Mexico (e-mail: caguilar@citedi.mx; moreno@citedi.mx; emorenov@ipn.mx).

Color versions of one or more of the figures in this paper are available online at http://ieeexplore.ieee.org.

Digital Object Identifier 10.1109/TMECH.2015.2485942

is designed to keep the error trajectories uniformly ultimately bounded (UUB). To show that this objective is satisfied, we prove that the asymptotic convergence of the output implies that the error state trajectories are bounded, which is achieved by introducing a rigorous analysis of the internal dynamics. The second contribution consists of a detailed real-time experimental study. Specifically, three controllers, including the proposed one, are experimentally tested. Using the same set of control gains for each controller, the performance is analyzed for both "slow" and "fast" periodic reference trajectories. The results show that the new controller exhibits the best performance for both tracking of the arm and regulation of the pendulum.

This paper is organized as follows. The Furuta pendulum dynamics and the control problem formulation are given in Section II. A new controller is proposed in Section III. The ultimate boundedness analysis for the error state trajectories is presented in Section IV. In Section V, with the aim to compare the real-time performance of the new controller, a PID controller is presented. Furthermore, a modified version of the output tracking controller introduced in [41] is also given. In Section VI, using an original testbed which has been accurately identified, the real-time experimental tests are presented, as well as the performance comparison are done. Finally, some concluding remarks are provided in Section VII.

## II. System Model and Control Problem Formulation

### A. Furuta Pendulum Dynamic Model and Error Model

As described previously, the Furuta pendulum is a mechanism consisting of an arm rotating in the horizontal plane and pendulum rotating in the vertical plane. See Fig. 1 for a description of the relative joint angle measurements and torque application.

The dynamic model of the Furuta pendulum in Euler-Lagrange form can be written as [4], [45], [46]:

$$M(\boldsymbol{q})\ddot{\boldsymbol{q}} + C(\boldsymbol{q},\dot{\boldsymbol{q}})\dot{\boldsymbol{q}} + \boldsymbol{g}(\boldsymbol{q}) + \boldsymbol{f}_v(\dot{\boldsymbol{q}}) + \boldsymbol{f}_c(\dot{\boldsymbol{q}}) = \boldsymbol{u} \tag{1}$$

where $\boldsymbol{q} = [\,q_1 \;\; q_2\,]^T$ is the vector of joint position, $\boldsymbol{u} = [\,\tau \;\; 0\,]^T$ is the input vector, being $\tau \in \mathbb{R}$ the torque input of the arm

$$M(\boldsymbol{q}) = \begin{bmatrix} \theta_1 + \theta_2 \sin^2(q_2) & \theta_3 \cos(q_2) \\ \theta_3 \cos(q_2) & \theta_4 \end{bmatrix}$$

$$C(\boldsymbol{q},\dot{\boldsymbol{q}}) = \begin{bmatrix} \frac{1}{2}\theta_2 \dot{q}_2 \sin(2q_2) & -\theta_3 \dot{q}_2 \sin(q_2) + \frac{1}{2}\theta_2 \dot{q}_1 \sin(2q_2) \\ -\frac{1}{2}\theta_2 \dot{q}_1 \sin(2q_2) & 0 \end{bmatrix}$$

$$\boldsymbol{g}(\boldsymbol{q}) = \begin{bmatrix} 0 \\ -\theta_5 \sin(q_2) \end{bmatrix}, \; \boldsymbol{f}_v(\dot{\boldsymbol{q}}) = \begin{bmatrix} \theta_6 \dot{q}_1 \\ \theta_7 \dot{q}_2 \end{bmatrix}$$

$$\boldsymbol{f}_c(\dot{\boldsymbol{q}}) = \begin{bmatrix} \theta_8 \tanh(\beta \dot{q}_1) \\ \theta_9 \tanh(\beta \dot{q}_2) \end{bmatrix}$$

where $M(\boldsymbol{q}) \in \mathbb{R}^{2\times 2}$ is the positive definite inertia matrix and $C(\boldsymbol{q},\dot{\boldsymbol{q}})\dot{\boldsymbol{q}} \in \mathbb{R}^2$ is the centrifugal and Coriolis torque vector,

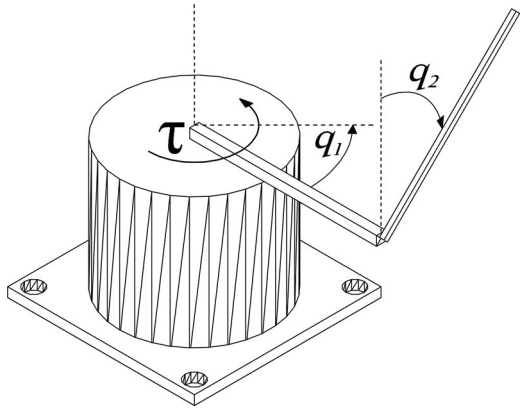


Fig. 1. Furuta pendulum sketch with relative joint angle measurements and torque application.

$\boldsymbol{g}(\boldsymbol{q}) \in \mathbb{R}^2$ is known as the gravitational torque vector, $\boldsymbol{f}_v(\dot{\boldsymbol{q}}) \in \mathbb{R}^2$ is the vector containing the viscous friction terms of each joint, and $\boldsymbol{f}_c(\dot{\boldsymbol{q}}) \in \mathbb{R}^2$ is a continuous and differentiable version of the Coulomb friction vector with $\beta > 0$ sufficiently large. Finally, $\theta_i$ with $i = \{1, .., 9\}$, are positive constant parameters related to the physical characteristics of the Furuta pendulum model.

In order to make easier the derivation of the control law, the open-loop dynamics in (1) is expressed as

$$\frac{d}{dt}\dot{\boldsymbol{q}} = \boldsymbol{f}_z(\boldsymbol{q},\dot{\boldsymbol{q}}) + \boldsymbol{g}_z(\boldsymbol{q})\tau \tag{2}$$

where $\boldsymbol{f}_z(\boldsymbol{q},\dot{\boldsymbol{q}}) = [f_{z1} \; f_{z2}]^T$ is the part of the Furuta pendulum dynamics that is not related to the control input $\tau$, given by

$$\boldsymbol{f}_z(\boldsymbol{q},\dot{\boldsymbol{q}}) = M(\boldsymbol{q})^{-1}[-C(\boldsymbol{q},\dot{\boldsymbol{q}})\dot{\boldsymbol{q}} - \boldsymbol{g}(\boldsymbol{q}) - \boldsymbol{f}_v(\dot{\boldsymbol{q}}) - \boldsymbol{f}_c(\dot{\boldsymbol{q}})] \tag{3}$$

and $\boldsymbol{g}_z(\boldsymbol{q}) = [g_{z1} \; g_{z2}]^T$ is the part that is directly related to the control input, such that

$$\boldsymbol{g}_z(\boldsymbol{q}) = \frac{1}{\det M}\begin{bmatrix} M_{22} \\ -M_{12} \end{bmatrix}. \tag{4}$$

By defining the tracking error vector as

$$\boldsymbol{e} = \begin{bmatrix} e_1 \\ e_2 \end{bmatrix} = \begin{bmatrix} q_{d1} - q_1 \\ q_{d2} - q_2 \end{bmatrix} \tag{5}$$

where $q_{d1}(t)$ is a twice-differentiable signal that denotes the desired trajectory for the position of the arm, and $q_{d2}$ is selected to be equal to zero. The open-loop error dynamics can be written as

$$\frac{d}{dt}\boldsymbol{x} = \boldsymbol{f}(t,\boldsymbol{x}) + \boldsymbol{g}(\boldsymbol{x})\tau \tag{6}$$

where

$$\boldsymbol{f}(t,\boldsymbol{x}) = \begin{bmatrix} \dot{e}_1 \\ \dot{e}_2 \\ \ddot{q}_{d1} - f_{z1} \\ -f_{z2} \end{bmatrix}, \; \boldsymbol{g}(\boldsymbol{x}) = \begin{bmatrix} 0 \\ 0 \\ -g_{z1} \\ -g_{z2} \end{bmatrix}, \text{ and } \boldsymbol{x} = \begin{bmatrix} e_1 \\ e_2 \\ \dot{e}_1 \\ \dot{e}_2 \end{bmatrix}.$$

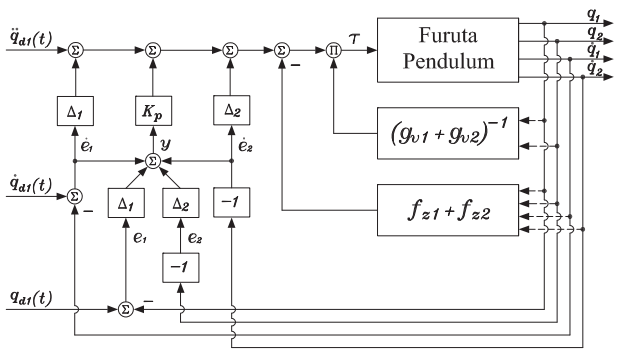


Fig. 2. Block diagram implementation of the feedback linearization based controller for the trajectory tracking of the Furuta pendulum.

### B. Control Problem

Let us consider that the desired trajectory $q_{d1}(t)$ is a smooth and twice-differentiable function, bounded in the sense

$$|q_{d1}(t)|,\ |\dot{q}_{d1}(t)|,\ |\ddot{q}_{d1}(t)| \leq \delta,\ \forall\, t \geq 0 \tag{7}$$

where $\delta$ is a positive constant.

The control problem consists in designing a controller $\tau \in \mathbb{R}$, such that the error trajectories $\boldsymbol{x}(t) \in \mathbb{R}^4$ satisfies the definition of a UUB signal. In other words, the controller should guarantee

$$\|\boldsymbol{x}(t_0)\| \leq a \ \ \Rightarrow \ \ \|\boldsymbol{x}(t)\| \leq b\ \ \forall\, t \geq t_0 + T \tag{8}$$

with $T = T(a,b) \geq 0$.

## III. Design of the Proposed Scheme

Feedback linearization technique is a control strategy well studied in, e.g., [43] and [44]. In this section, a novel application of this control technique is developed, designing a new tracking controller for the Furuta pendulum system.

The output of the system (6) is proposed as a function that depends on the full error state $\boldsymbol{x}$, this is

$$y = \Delta_1 e_1 + \Delta_2 e_2 + \dot{e}_1 + \dot{e}_2 \tag{9}$$

where $\Delta_1$ and $\Delta_2$ are positive constants. The time derivative of the output function $y(t)$ is given by

$$\frac{d}{dt}y = \ddot{q_{d1}} - f_{z1} - f_{z2} + \Delta_1 \dot{e}_1 + \Delta_2 \dot{e}_2 - [g_{z1} + g_{z2}]\tau. \tag{10}$$

Then, the control input which linearizes the output dynamics in (10) is given by

$$\tau = \frac{-\Delta_1 \dot{e}_1 - \Delta_2 \dot{e}_2 - \ddot{q}_{d1} + f_{z1} + f_{z2} - K_p y}{-[g_{z1} + g_{z2}]} \tag{11}$$

where $K_p$ is a positive constant, $f_{z1}$ and $f_{z2}$ are defined in (3), and $g_{z1}$ and $g_{z2}$ are defined in (4). The block diagram implementation of the controller in (11) is shown in Fig. 2.

Note that the system (6) is relative degree one with the proposed output function in (9) and the closed-loop dynamics in terms of the output $y$ can be written as

$$\frac{d}{dt}y = -K_p y \tag{12}$$

which delivers

$$\lim_{t\to\infty} y(t) = 0 \tag{13}$$

with exponential convergence rate.

It is worth mentioning that the controller (11) is valid in a region of the state space where $g_{z1} + g_{z2} \neq 0$. However, for the case of the Furuta pendulum we have

$$g_{z1} + g_{z2} < 0,\ \forall\, |q_2| < \arccos(\theta_4/\theta_3). \tag{14}$$

In the experimental study presented in this paper, the inequality (14) is satisfied for all time $t \geq 0$. See Section VI for the numeric values of the parameters $\theta_3$ and $\theta_4$.

## IV. Ultimate Boundedness Analysis

When a feedback linearization controller is applied, more specifically, an input–output linearization controller, it is necessary to study the internal dynamics of the system. By means of input–output linearization, the dynamics of a nonlinear system is decomposed into an external (input–output) part and an internal (unobservable) part.

For obtaining the internal dynamics, it is necessary to define a coordinate transformation vector $\boldsymbol{z} = [\boldsymbol{\eta}^T\ \zeta_1]^T \in \mathbb{R}^4$, where $\zeta_1$ is the output function and the vector $\boldsymbol{\eta} \in \mathbb{R}^3$ satisfies the partial differential equation system

$$L_g \eta_i = \frac{\partial \eta_i}{\partial \boldsymbol{x}}\, \boldsymbol{g}(\boldsymbol{x}) = 0, \qquad i = 1,2,3 \tag{15}$$

with $\boldsymbol{g}(\boldsymbol{x})$ is defined in (6).

The proposed transformation is given by

$$\boldsymbol{z} = \begin{bmatrix} \eta_1 \\ \eta_2 \\ \eta_3 \\ \zeta_1 \end{bmatrix} = H\boldsymbol{x} = \begin{bmatrix} 1 & 0 & 0 & 0 \\ 0 & 1 & 0 & 0 \\ 0 & 0 & -\frac{g_{z2}}{g_{z1}} & 1 \\ \Delta_1 & \Delta_2 & 1 & 1 \end{bmatrix} \begin{bmatrix} e_1 \\ e_2 \\ \dot{e}_1 \\ \dot{e}_2 \end{bmatrix} \tag{16}$$

and the inverse transformation is given by

$$\boldsymbol{x} = H^{-1}\boldsymbol{z} = \begin{bmatrix} 1 & 0 & 0 & 0 \\ 0 & 1 & 0 & 0 \\ -\Delta_1 G_1 & -\Delta_2 G_1 & -G_1 & G_1 \\ -\Delta_1 G_2 & -\Delta_2 G_2 & G_1 & G_2 \end{bmatrix} \begin{bmatrix} \eta_1 \\ \eta_2 \\ \eta_3 \\ \zeta_1 \end{bmatrix} \tag{17}$$

where

$$G_1 = \frac{g_{z1}}{g_{z1} + g_{z2}},\ G_2 = \frac{g_{z2}}{g_{z1} + g_{z2}}.$$

The overall closed-loop system corresponds to the system of differential equations given by

$$\frac{d}{dt}\begin{bmatrix} \boldsymbol{\eta} \\ \zeta_1 \end{bmatrix} = \begin{bmatrix} \boldsymbol{w}(t, \zeta_1, \boldsymbol{\eta}) \\ -K_p \zeta_1 \end{bmatrix}. \tag{18}$$

The explicit expression of the internal dynamics of the Furuta pendulum is obtained by calculating the time derivative of $\boldsymbol{\eta}$

in (16). Therefore, by substituting $\ddot{e}_1$ and $\ddot{e}_2$ from the open-loop error dynamics in (6), using $\dot{e}_1$ and $\dot{e}_2$ from the inverse transformation in (17), and substituting $g_{z1}$ and $g_{z2}$ obtained from (4), the internal dynamics can be expressed as

$$\dot{\boldsymbol{\eta}} = \begin{bmatrix} -\Delta_1 G_1 \eta_1 - \Delta_2 G_1 \eta_2 - G_1 \eta_3 + G_1 \zeta_1 \\ -\Delta_1 G_2 \eta_1 - \Delta_2 G_2 \eta_2 + G_1 \eta_3 + G_2 \zeta_1 \\ \dfrac{\theta_3}{\theta_4}\cos(\eta_2)\ddot{q}_{d1} - \dfrac{\theta_3}{\theta_4}\cos(\eta_2) f_{z1} - \dfrac{\theta_3}{\theta_4}\sin(\eta_2)\dot{\eta}_1\dot{\eta}_2 - f_{z2} \end{bmatrix}. \tag{19}$$

The internal dynamics in (19) and the external dynamics in (12) provide an explicit expression of the overall closed-loop system (18).

An important remark is that the internal dynamics (19) can be rewritten as

$$\dot{\boldsymbol{\eta}} = \boldsymbol{w}_1(\zeta_1, \boldsymbol{\eta}) + \boldsymbol{w}_2(t, \zeta_1, \boldsymbol{\eta}) \tag{20}$$

where $\boldsymbol{w}_1(\zeta_1, \boldsymbol{\eta}) \in \mathbb{R}^3$ is the part of the internal dynamics that is not related to the desired trajectory $q_{d1}(t)$, and $\boldsymbol{w}_2(t, \zeta_1, \boldsymbol{\eta}) \in \mathbb{R}^3$ are the disturbances due to the tracking of $q_{d1}(t)$, that is, the part of the internal dynamics that is related to the desired trajectory. It is noteworthy that, if the desired trajectory $q_{d1}$ is constant, then the function $\boldsymbol{w}_2 = 0$. The explicit expression of the functions $\boldsymbol{w}_1(\zeta_1, \boldsymbol{\eta})$ and $\boldsymbol{w}_2(t, \zeta_1, \boldsymbol{\eta})$ can be obtained from (19) and are given in Appendix A.

Let us observe that the internal dynamics (20) can be manipulated as follows:

$$\dot{\boldsymbol{\eta}} = A\boldsymbol{\eta} + \boldsymbol{w}_2(t, 0, \boldsymbol{\eta}) + \boldsymbol{\sigma} + \boldsymbol{\Psi} \tag{21}$$

where $A\boldsymbol{\eta}$ is the linearization of $\boldsymbol{w}_1(0, \boldsymbol{\eta})$ around the origin, with the constant matrix $A \in \mathbb{R}^{3\times 3}$ defined as

$$A = \frac{\partial \boldsymbol{w}_1(0, \boldsymbol{\eta})}{\partial \boldsymbol{\eta}}|_{\boldsymbol{\eta}=0} \tag{22}$$

the function $\boldsymbol{\sigma}$ is the error between the internal dynamics and zero-dynamics, which is given by

$$\boldsymbol{\sigma} = \boldsymbol{w}_1(\zeta_1, \boldsymbol{\eta}) + \boldsymbol{w}_2(t, \zeta_1, \boldsymbol{\eta}) - [\boldsymbol{w}_1(0, \boldsymbol{\eta}) + \boldsymbol{w}_2(t, 0, \boldsymbol{\eta})] \tag{23}$$

and the function $\boldsymbol{\Psi}$ is defined as the disturbance term due to the dynamics neglected by the linearization of $\boldsymbol{w}_1(0, \boldsymbol{\eta})$, given by

$$\boldsymbol{\Psi}(\boldsymbol{\eta}) = \boldsymbol{w}_1(0, \boldsymbol{\eta}) - A\boldsymbol{\eta}. \tag{24}$$

Note that $\boldsymbol{\Psi}(0) = 0$.

In the following, some properties of the functions $\boldsymbol{\sigma}$, $\boldsymbol{\Psi}$, and $\boldsymbol{w}_2$ are introduced in preparation for stating our main results.

Defining the set

$$B_r = \{\boldsymbol{z} \in \mathbb{R}^4 \mid \|\boldsymbol{z}\| \leq r\} \tag{25}$$

it is possible to state the following property.

*Property 1:* The function $\boldsymbol{\sigma}(t, \boldsymbol{z}) : \mathbb{R} \times \mathbb{R}^4 \to \mathbb{R}^3$ satisfies

$$\|\boldsymbol{\sigma}(t, \boldsymbol{z})\| \leq k_0 |\zeta_1|, \ \forall\, \boldsymbol{z} \in B_r, \ t \geq 0 \tag{26}$$

where $k_0$ is the Lipschitz constant and $B_r$ is given in (25).

*Proof:* Given that $\boldsymbol{\sigma}(t, \boldsymbol{z})$ is a smooth and differentiable function, it is at least locally Lipschitz. Thus, by the mean value theorem, for any $B_r$ there is a proper $k_0$ such that

$$\|\boldsymbol{\sigma}(t, \boldsymbol{z}_1) - \boldsymbol{\sigma}(t, \boldsymbol{z}_2)\| \leq k_0 \|\boldsymbol{z}_1 - \boldsymbol{z}_2\| \tag{27}$$

where $k_0$ can be estimated as

$$k_0 = \max_{\substack{\boldsymbol{z} \in B_r \\ \forall \\ t \in \mathbb{R}^+}} \left\| \frac{\partial \boldsymbol{\sigma}(t, \boldsymbol{z})}{\partial \boldsymbol{z}} \right\|$$

based on the assumption (7). □

By choosing $\boldsymbol{z}_1 = [\boldsymbol{\eta}^T \ \zeta_1]^T$ and $\boldsymbol{z}_2 = [\boldsymbol{\eta}^T \ 0] \in \mathbb{R}^4$, the inequality (27) can be further rewritten as

$$\begin{aligned} \|\boldsymbol{\sigma}(t, \boldsymbol{z}_1) - \boldsymbol{\sigma}(t, \boldsymbol{z}_2)\| &= \|\boldsymbol{\sigma}(t, \zeta_1, \boldsymbol{\eta})\| \\ &\leq k_0 \left\| \begin{bmatrix} \boldsymbol{\eta} \\ \zeta_1 \end{bmatrix} - \begin{bmatrix} \boldsymbol{\eta} \\ 0 \end{bmatrix} \right\| \\ &= k_0 |\zeta_1|. \end{aligned}$$

*Property 2:* The function $\boldsymbol{\Psi}(\boldsymbol{\eta}) : \mathbb{R}^3 \to \mathbb{R}^3$ in (24) satisfies

$$\|\boldsymbol{\Psi}(\boldsymbol{\eta})\| \leq c_0 \|\boldsymbol{\eta}\|, \ \forall\, \boldsymbol{\eta} \in B_0, \tag{28}$$

where $c_0$ is a positive constant, $B_0 = \{B_r \cap \{\zeta_1 = 0\}\}$, and $B_r$ is given in (25).

*Proof:* Using the Mean Value Theorem for $\boldsymbol{\Psi}(\boldsymbol{\eta})$, one obtains

$$\boldsymbol{\Psi}(\boldsymbol{x}) - \boldsymbol{\Psi}(\boldsymbol{y}) = \left.\frac{\partial \boldsymbol{\Psi}(\boldsymbol{s})}{\partial \boldsymbol{s}}\right|_{\boldsymbol{s}=\boldsymbol{c}} [\boldsymbol{x} - \boldsymbol{y}]$$

and assuming $\boldsymbol{y} = 0$,

$$\begin{aligned} \|\boldsymbol{\Psi}(\boldsymbol{x})\| &= \left\| \left.\frac{\partial \boldsymbol{\Psi}(\boldsymbol{s})}{\partial \boldsymbol{s}}\right|_{\boldsymbol{s}=\boldsymbol{c}} [\boldsymbol{x}] \right\| \leq c_0 \|\boldsymbol{x}\| \\ c_0 &= \max_{\forall \boldsymbol{s} \in B_0} \left\| \frac{\partial \boldsymbol{\Psi}(\boldsymbol{s})}{\partial \boldsymbol{s}} \right\|. \end{aligned}$$

□

*Property 3:* The function $\boldsymbol{w}_2(t, 0, \boldsymbol{\eta}) \in \mathbb{R}^3$ satisfies

$$\|\boldsymbol{w}_2(t, 0, \boldsymbol{\eta})\| \leq c_1, \ \forall\, \boldsymbol{\eta} \in B_0, \ t \geq 0 \tag{29}$$

where $c_1$ is a positive constant, $B_0 = \{B_r \cap \{\zeta_1 = 0\}\}$, and $B_r$ is given in (25), based on the assumption (7).

We are now in a position to establish our main results.

*Proposition 1:* The solutions of $\boldsymbol{z}(t) = [\boldsymbol{\eta}(t)^T \ \zeta_1(t)]^T \in \mathbb{R}^n$ of the closed-loop system (18) are UUB.

*Proof:* A positive definite function is proposed as

$$V = \frac{1}{2}\zeta_1^2 + \epsilon \frac{1}{2} \boldsymbol{\eta}^T P \boldsymbol{\eta} \tag{30}$$

where $P$ satisfies the Lyapunov equation [43]:

$$\frac{1}{2}[PA + A^T P] = -Q \tag{31}$$

for $A$ defined as (22), and known to be Hurwitz (See Appendix A for the proof of this fact).

The time derivative of $V$ along (21) is given by

$$\begin{aligned}\dot{V} =& -K_p\zeta_1^2 + \epsilon\boldsymbol{\eta}^T\left[\frac{1}{2}[PA + A^TP]\right]\boldsymbol{\eta} + \epsilon\boldsymbol{\eta}^TP\boldsymbol{w}_2(t,0,\boldsymbol{\eta}) \\ &+\epsilon\boldsymbol{\eta}^TP\boldsymbol{\Psi} + \epsilon\boldsymbol{\eta}^TP\boldsymbol{\sigma} \qquad (32)\\ =& -K_p\zeta_1^2 - \epsilon\boldsymbol{\eta}^TQ\boldsymbol{\eta} + \epsilon\boldsymbol{\eta}^TP\boldsymbol{w}_2(t,0,\boldsymbol{\eta}) \\ &+\epsilon\boldsymbol{\eta}^TP\boldsymbol{\Psi} + \epsilon\boldsymbol{\eta}^TP\boldsymbol{\sigma}. \qquad (33)\end{aligned}$$

Considering the bounds in (28), (26), and (29), the terms of $\dot{V}$ in (33) satisfy the following inequalities:

$$\begin{aligned}-\epsilon\boldsymbol{\eta}^TQ\boldsymbol{\eta} &\le -\epsilon\lambda_{\min}\{Q\}\|\boldsymbol{\eta}\|^2 \qquad (34)\\ \epsilon\boldsymbol{\eta}^TP\boldsymbol{\sigma} &\le \epsilon k_0\|P\||\zeta_1|\|\boldsymbol{\eta}\| \qquad (35)\\ \epsilon\boldsymbol{\eta}^TP\boldsymbol{\Psi} &\le \epsilon c_0\|P\|\|\boldsymbol{\eta}\|^2 \qquad (36)\\ \epsilon\boldsymbol{\eta}^TP\boldsymbol{w}_2(t,0,\boldsymbol{\eta}) &\le \epsilon c_1\|P\|\|\boldsymbol{\eta}\|. \qquad (37)\end{aligned}$$

Using the inequalities defined in (34)–(37), the function $\dot{V}$ can be bounded as

$$\begin{aligned}\dot{V} \le& -K_p\zeta_1^2 - \epsilon\lambda_{\min}\{Q\}\|\boldsymbol{\eta}\|^2 + \epsilon c_1\|P\|\|\boldsymbol{\eta}\| \\ &+\epsilon c_0\|P\|\|\boldsymbol{\eta}\|^2 + \epsilon k_0\|P\||\zeta_1|\|\boldsymbol{\eta}\| \\ \le& -K_p\zeta_1^2 - \epsilon[\lambda_{\min}\{Q\} - c_0\|P\|]\|\boldsymbol{\eta}\|^2 \\ &+\epsilon c_1\|P\|\left\|\begin{bmatrix}\|\boldsymbol{\eta}\| \\ |\zeta_1|\end{bmatrix}\right\| + \epsilon k_0\|P\||\zeta_1|\|\boldsymbol{\eta}\| \\ \le& -\begin{bmatrix}\|\boldsymbol{\eta}\| \\ |\zeta_1|\end{bmatrix}^T Q_0\begin{bmatrix}\|\boldsymbol{\eta}\| \\ |\zeta_1|\end{bmatrix} + \epsilon c_1\|P\|\left\|\begin{bmatrix}\|\boldsymbol{\eta}\| \\ |\zeta_1|\end{bmatrix}\right\| \\ \le& -\lambda_{\min}\{Q_0\}\,\|\boldsymbol{z}\|^2 + \epsilon c_1\|P\|\,\|\boldsymbol{z}\| \qquad (38)\end{aligned}$$

where $\boldsymbol{z}$ is defined in (16) and

$$Q_0 = \begin{bmatrix}\epsilon[\lambda_{\min}\{Q\} - c_0\|P\|] & -\frac{1}{2}\epsilon\|P\|k_0 \\ -\frac{1}{2}\epsilon\|P\|k_0 & K_p\end{bmatrix}. \qquad (39)$$

Using a part of $-\lambda_{\min}\{Q_0\}\|\boldsymbol{z}\|^2$ to dominate $\epsilon c_1\|P\|\|\boldsymbol{z}\|$ for sufficiently large values of $\|\boldsymbol{z}\|$, we rewrite the inequality (38) as

$$\dot{V} \le -(\lambda_{\min}\{Q_0\} - \gamma)\|\boldsymbol{z}\|^2 - \gamma\|\boldsymbol{z}\|^2 + \epsilon c_1\|P\|\|\boldsymbol{z}\| \qquad (40)$$

being $0 < \gamma < \lambda_{\min}\{Q_0\}$ a positive constant, such that

$$\dot{V} \le -(\lambda_{\min}\{Q_0\} - \gamma)\|\boldsymbol{z}\|^2, \;\; \forall\mu \le \|\boldsymbol{z}\| \le r \qquad (41)$$

where

$$\mu = \epsilon c_1\|P\|\gamma^{-1} \qquad (42)$$

and $r > \mu$ introduced in the definition of the region $B_r$ in (25).

Thus, one obtains $\dot{V} < 0$ for $\|\boldsymbol{z}\| \ge \mu$. Therefore, in agreement to Theorem 4.18, page 172 in [43], it is possible to conclude that the solutions $\boldsymbol{\eta}(t)$ and $\zeta_1(t)$ are UUB. □

It is possible to prove that if $q_{d1}(t)$ is constant, then the constant $c_1$ related to the Property 3 in (29) can be selected as zero, and the result stated in Proposition 1 becomes one of asymptotic stability.

### A. Ultimate Bound

The ultimate bound of the solutions $\boldsymbol{z}(t)$ is computed as follows. Lower and upper bounds of the function $V$ in (31) are given by

$$\begin{aligned}V(\boldsymbol{z}) &\ge \alpha_1(\|\boldsymbol{z}\|) = \lambda_{\min}\{P_v\}\|\boldsymbol{z}\|^2 \qquad (43)\\ V(\boldsymbol{z}) &\le \alpha_2(\|\boldsymbol{z}\|) = \lambda_{\max}\{P_v\}\|\boldsymbol{z}\|^2 \qquad (44)\end{aligned}$$

respectively, where

$$P_v = \begin{bmatrix}\frac{\epsilon P}{2} & 0 \\ 0 & \frac{1}{2}\end{bmatrix}.$$

Thus, in agreement to Theorem 4.18, page 172 in [43], the ultimate bound on $\boldsymbol{z}(t)$ can be calculated as

$$\|\boldsymbol{z}\| \le b = \alpha_1^{-1}(\alpha_2(\mu)) = \sqrt{\frac{\lambda_{\max}\{P_v\}\mu^2}{\lambda_{\min}\{P_v\}}} \qquad (45)$$

with $\mu$ defined in (42). Note that the constant $r$ involved in the set $B_r$ defined in (25) should satisfy $r > b$. This guarantees the existence of a positively invariant set $\Omega_c = \{V(\boldsymbol{z}) \le c = \alpha_1(r)\}$, such that for every $\boldsymbol{z}(t_0)$ starting in $\Omega_c$, the trajectories $\boldsymbol{z}(t)$ will enter in the set $\Omega_\varepsilon = \{V(\boldsymbol{z}) \le \varepsilon = \alpha_2(\mu)\}$, with $\varepsilon < c$. This means that Properties 1–3 are valid in a region bigger than the ultimate bound $b$ in (45). For further discussion see also Section 4.8, page 168 of [43].

### B. Boundedness of the Error Trajectories

*Proposition 2:* Given that the solutions of $\boldsymbol{z}(t) = [\boldsymbol{\eta}(t)^T\;\zeta_1(t)]^T \in \mathbb{R}^n$ are UUB, the solutions of the error dynamics of the Furuta pendulum $\boldsymbol{x}(t) = [e_1(t)\;e_2(t)\;\dot{e}_1(t)\;\dot{e}_2(t)]^T \in \mathbb{R}^n$ are UUB as well.

*Proof:* Given that

$$\boldsymbol{x}(t) = H^{-1}(t)\begin{bmatrix}\boldsymbol{\eta}(t) \\ \zeta_1(t)\end{bmatrix} \qquad (46)$$

then, an upper bound to the state vector $\boldsymbol{x}(t)$ can be expressed as

$$\|\boldsymbol{x}(t)\| \le \|H^{-1}(t)\|\left\|\begin{bmatrix}\boldsymbol{\eta}(t) \\ \zeta_1(t)\end{bmatrix}\right\|. \qquad (47)$$

Therefore, it is possible to conclude that the state vector $\boldsymbol{x}(t) = [e_1(t)\;e_2(t)\;\dot{e}_1(t)\;\dot{e}_2(t)]^T$ is UUB as well.

Note that the condition to guarantee that $\|H^{-1}\|$ is bounded above and below is

$$\det(H) = \frac{\theta_3}{\theta_4}\cos(e_2) - 1 \neq 0$$

which also provides a guideline to select the value of $r$ in order satisfy the Properties 1–3, resulting in

$$r < \arccos(\theta_4/\theta_3) = 0.7839\;[\text{rad}]$$

for our experimental system.

It is possible to show that a sufficient condition for the trajectories $\boldsymbol{\eta}(t)$ to be UUB is that

$$\Delta_2 > \kappa_2(\theta_i, \Delta_1) \tag{48}$$

where $\kappa_2(\theta_i, \Delta_1)$ is a function of the Furuta pendulum parameters $\theta_i$, which are constants, and of the control gain $\Delta_1$. The above statement can be inferred from the proof of Proposition 1, where (31) requires that the matrix $A$ be Hurwitz, and in Appendix A we show that the inequality in (48) is a sufficient condition to ensure that matrix $A$ is Hurwitz. In fact, the inequality in (48) provides an explicit tuning guideline, which consists in selecting $\Delta_2$ sufficiently large. See Appendix A for the explicit expression of the right-hand side of (48).

## V. Controllers for the Performance Comparison

In this section, two additional controllers for the trajectory tracking of the Furuta pendulum are presented. This is in order to make a comparison of the performance between the proposed feedback linearization controller and the controllers in this section. Firstly, a PID controller for the trajectory tracking of the Furuta pendulum is presented. Secondly, an output tracking nonlinear controller is presented, which is reported in [41].

### A. PID Controller

We introduce a PID tracking controller for the Furuta pendulum, where the PD part is tuned by pole placement following the state feedback procedure.

Consider that the control input given by

$$\tau = -K_{\mathrm{PD}}\boldsymbol{x} \tag{49}$$

with $K_{\mathrm{PD}} = [k_{p1}\ k_{p2}\ k_{d1}\ k_{d2}]$ being a vector of positive constants, applied to the system (6) leads to the closed-loop linear dynamics

$$\frac{d}{dt}\boldsymbol{x} = A^*\boldsymbol{x} \tag{50}$$

where, taking into account that $q_{d1} = 0$, $\boldsymbol{f}(t, 0) = 0$, and

$$\frac{\partial}{\partial \boldsymbol{x}}\boldsymbol{g}(\boldsymbol{x})\bigg|_{\boldsymbol{x}=0} = 0$$

the matrix $A^* \in \mathbb{R}^{4\times 4}$ is given by

$$A^* = \frac{\partial}{\partial \boldsymbol{x}}\boldsymbol{f}(t, \boldsymbol{x})\bigg|_{\boldsymbol{x}=0} - \boldsymbol{g}(0)K_{\mathrm{PD}}. \tag{51}$$

In addition, let us introduce the integral of the error term $\boldsymbol{\xi} = [\xi_1\ \xi_2]^T$, defined as

$$\frac{d}{dt}\boldsymbol{\xi} = \boldsymbol{e} \tag{52}$$

with $\boldsymbol{e}(t)$ given in (5), such that the final PID control action is expressed as

$$\tau = -K_{\mathrm{PD}}\boldsymbol{x} - K_{\mathrm{I}}\boldsymbol{\xi} \tag{53}$$

where $K_{\mathrm{I}} = [k_{i1}\ k_{i2}]$ is a vector of positive constants.

### B. Output Tracking Controller

In [41], an output tracking controller is derived from a particular case of the Furuta pendulum parameters, where the joint frictions and pendulum inertia are neglected. In order to apply the design procedure presented in [41], using the dynamic model in (1) and considering that the pendulum inertia is negligible, the condition

$$\theta_2 = \theta_4 \tag{54}$$

where $\theta_2$ and $\theta_4$ are constant parameters of the dynamic model in (1), is required. In other words, the condition (54) has been used to implement the controller [41] in our platform.

Considering the output function $Z(\boldsymbol{q})$ for the output tracking controller defined as

$$Z = r^* q_1 + h\sin(q_2) \tag{55}$$

and following the design procedure presented in [41], it is possible to obtain the output tracking controller with friction compensation

$$\begin{aligned}\tau = {} & \theta_2 G(q_2)\sin(q_2)\cos^2(q_2)\dot{q}_1^2 + \theta_5 G(q_2)\sin(q_2)\cos(q_2) \\ & -G(q_2)\cos(q_2)\theta_7\dot{q}_2 - G(q_2)\cos(q_2)\theta_9\tanh(\beta\dot{q}_2) \\ & +\theta_6\dot{q}_1 + \theta_8\tanh(\beta\dot{q}_1) + [N(q_2)h - \theta_3]\sin(q_2)\dot{q}_2^2 \\ & +\theta_2\sin(2q_2)\dot{q}_1\dot{q}_2 - K_1 N(q_2)\dot{Z} \\ & -K_2 N(q_2)Z + N(q_2)v\end{aligned} \tag{56}$$

where

$$\begin{aligned}G(q_2) = {} & \frac{[\theta_1 + \theta_2\sin^2(q_2)]h - \theta_3 r^*}{\theta_3 h\cos^2(q_2) - \theta_2 r^*}, \\ N(q_2) = {} & \frac{1}{r^*}[[\theta_1 + \theta_2\sin^2(q_2)] - G(q_2)\theta_3\cos^2(q_2)], \\ v = {} & \ddot{Z}_d + K_1\dot{Z}_d + K_2 Z_d - K_3\dot{q}_2\end{aligned}$$

with $r^*$, $h$, $K_1$, $K_2$, and $K_3$ being positive constants, and $Z_d(t)$ the desired output trajectory. Note that the controller in (56) corresponds to the one presented in [41], but terms of viscous friction and Coulomb friction have been incorporated to its development, with the aim of improving the experimental performance.

## VI. Experimental Evaluation

### A. Experimental Platform

In this section, the real-time implementation of the proposed controller (11) is presented, as well as the implementation of the PID controller in (53) and the output tracking controller with friction compensation in (56). In additon, we present a performance comparison between these control schemes. The experimental tests have been conducted in a Furuta pendulum prototype built in Instituto Politécnico Nacional-CITEDI. See Fig. 3 for picture of the experimental system.

The hardware components used for the instrumentation and control of the Furuta pendulum experimental platform were as follows:

1) Desktop personal computer (PC).
2) PCI data acquisition (DAQ) board Sensoray 626.

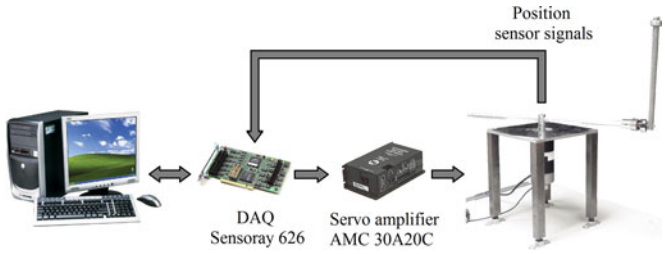


Fig. 3. General structure of the experimental platform of the Furuta pendulum built in Instituto Politécnico Nacional-CITEDI.

TABLE I
NUMERICAL VALUES OF THE FURUTA PENDULUM PARAMETERS

| Symbol | Value | Unit |
|---|---|---|
| $\theta_1$ | 0.0619 | $\mathrm{Kg}\cdot\mathrm{m}^2\cdot\mathrm{rad}$ |
| $\theta_2$ | 0.0149 | $\mathrm{Kg}\cdot\mathrm{m}^2\cdot\mathrm{rad}$ |
| $\theta_3$ | 0.0185 | $\mathrm{Kg}\cdot\mathrm{m}^2\cdot\mathrm{rad}$ |
| $\theta_4$ | 0.0131 | $\mathrm{Kg}\cdot\mathrm{m}^2\cdot\mathrm{rad}$ |
| $\theta_5$ | 0.5076 | $\mathrm{Kg}\cdot\mathrm{m}^2\cdot\mathrm{rad}$ |
| $\theta_6$ | 0.0083 | $\mathrm{N}\cdot\mathrm{m}\cdot\mathrm{rad/s}$ |
| $\theta_7$ | 0.0007 | $\mathrm{N}\cdot\mathrm{m}\cdot\mathrm{rad/s}$ |
| $\theta_8$ | 0.0188 | $\mathrm{N}\cdot\mathrm{m}\cdot\mathrm{rad/s}$ |
| $\theta_9$ | 0.0087 | $\mathrm{N}\cdot\mathrm{m}\cdot\mathrm{rad/s}$ |

3) Optical encoders Quantum Devices QD200-05/05-1000-4-03-T3-01-02.
4) Servo amplifier Advanced Motion Controls 30A20AC.
5) DC motor model MBR3410NI as actuator.

The PC runs Windows XP operative system, MATLAB 2007a and Simulink, which interacts with the DAQ through the Real-Time Windows Target libraries at $1\times10^{-3}$[s] sampling rate. Fig. 3 shows the block diagram that represents the general structure of the experimental platform aforementioned.

The constant parameters $\theta_i$ of the Furuta pendulum model in (1) have been identified. These parameters are shown in Table I, which were obtained by using the filtered dynamic model and the least squares identification algorithm. In the identification process, $\beta = 100$ was considered, which is related to the vector of Coulomb friction $\boldsymbol{f}_c(\dot{\boldsymbol{q}})$ in the Furuta pendulum model (1).

It is worth remarking that $q_1(t)$ denotes the angular position of the horizontal arm, where the application of a positive torque $\tau(t)$ produces a positive counterclockwise movement in the arm position. The signal $q_2(t)$ denotes the angular position of the pendulum measured with respect to the upward position and positive displacement is the clockwise sense, which means that the upward pendulum position is equivalent to zero radians. See Fig. 1 for a graphical description of the angle measurement. The initial conditions of the experimental system were null for every experiment presented in this paper, i.e., the pendulum is at the upward position when the experiment starts.

## B. Experimental Results

For the experimental evaluation and the performance comparison of the control schemes presented, the desired trajectory $q_{d1}(t)$ for the arm position was defined as

$$q_{d1}(t) = \sin(\omega t) \tag{57}$$

where two different values for the angular velocity $\omega$ were used, such that $\omega = 1$ [rad/s] was used for a comparison at low speed, and $\omega = 2.5$ [rad/s] was used for a comparison at high speed, which increases the nonlinear properties of the system. Particularly, for the output tracking controller in (56), for which the desired position is defined in relation with the desired output, the reference trajectory is defined by

$$q_{d1}(t) = \frac{Z_d(t)}{r^*} \tag{58}$$

$$Z_d(t) = r^*\sin(wt). \tag{59}$$

For convenience, we will use the notation $\tau_{\mathrm{fl}}$ for the proposed feedback linearization controller in (11), $\tau_{\mathrm{pid}}$ for the PID controller in (53), and $\tau_{\mathrm{ot}}$ for the output tracking algorithm in (56).

For the PD part of the PID controller $\tau_{\mathrm{pid}}$ in (53), the control gains $K_{\mathrm{PD}}$ were selected such that the poles of the closed-loop system (50) are located at $-7$, $-5$, $-5+5i$, and $-5-5i$. The resulting control gains were $k_{p1} = 1.62$, $k_{p2} = 8.1$, $k_{d1} = 0.89$, and $k_{d2} = 1.18$. Regarding the integral part, the control gains $K_{\mathrm{I}}$ were experimentally tuned, looking for an improvement in the performance of the PD part. These gains were selected as $k_{i1} = 0.17$ and $k_{i2} = 1.75$.

For the tuning of the nonlinear controllers $\tau_{\mathrm{fl}}$ in (11) and $\tau_{\mathrm{ot}}$ in (56), a torque-based guideline was used. Control gains with good performance were selected for each controller taking into account the RMS values of the applied torque for a selected time window $t_1 \le t \le t_2$, looking for a difference within 5% of this index between the proposed algorithm $\tau_{\mathrm{fl}}$ and the output tracking controller $\tau_{\mathrm{ot}}$. Thereby, the performance is evaluated for similar values of the energy applied by each nonlinear controller.

The control gains used for the output tracking controller with friction compensation $\tau_{\mathrm{ot}}$ in (56) were $r^* = 0.55$, $h = 0.6$, $K_1 = 6$, $K_2 = 8$, and $K_3 = 1$. The control gains concerning the feedback linearization controller $\tau_{\mathrm{fl}}$ in (11) were selected as $K_p = 2$, $\Delta_1 = 6$, $\Delta_2 = 8$. It is noteworthy that the values of $\Delta_1$ and $\Delta_2$ satisfy the condition in (48).

The experimental results for the three different control algorithms are illustrated in Figs. 4–6. Top plots depict the results for the tracking of $q_{d1}(t)$ with $\omega = 1$ [rad/s], while bottom plots show results for $\omega = 2.5$ [rad/s]. In particular, the Fig. 4 shows the time evolution of $q_1(t)$ and $q_{d1}(t)$, Fig. 5 depicts the time evolution of $q_2(t)$, and the applied torque is observed in Fig. 6.

Follow the link at [49] to see a video of the implementation of the feedback linearization controller in (11) by using the slow trajectory $q_{d1}(t)$, with $\omega = 1$. Similarly, the link at [50] shows the real-time experiment of the new controller by using the fast trajectory $q_{d1}(t)$ with $\omega = 2.5$.

The control actions obtained for the three controllers have high-frequency components. This is attributed to the PWM switching of the servo amplifier and the velocity estimation, which is obtained by using the "dirty" derivative algorithm [47]:

$$\dot{\boldsymbol{q}}(Tk) \approx \frac{\boldsymbol{q}(Tk) - \boldsymbol{q}(T[k-1])}{T} \tag{60}$$

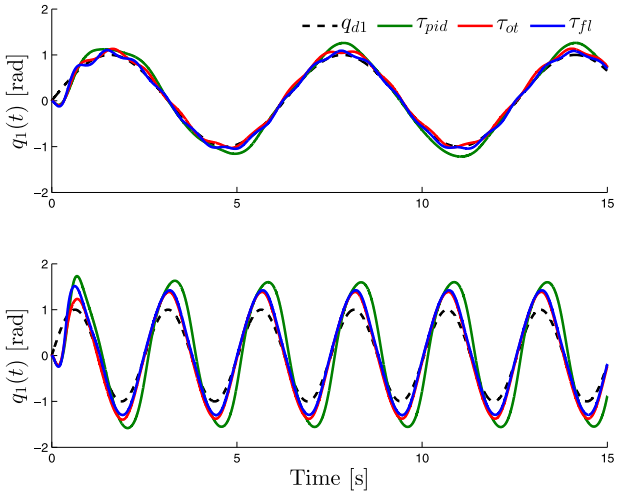


Fig. 4. Time evolution of the arm position $q_1(t)$ during the tracking of the desired trajectory $q_{d1}(t)$ obtained for $\tau_{\text{fl}}$, $\tau_{\text{ot}}$, and $\tau_{\text{pid}}$, with $\omega = 1$ (top) and $\omega = 2.5$ (bottom).

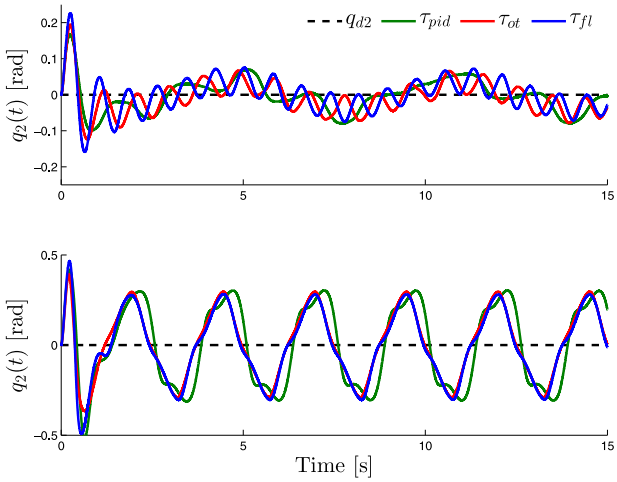


Fig. 5. Time evolution of the pendulum position $q_2(t)$ obtained for $\tau_{\text{fl}}$, $\tau_{\text{ot}}$, and $\tau_{\text{pid}}$, with $\omega = 1$ (top) and $\omega = 2.5$ (bottom).

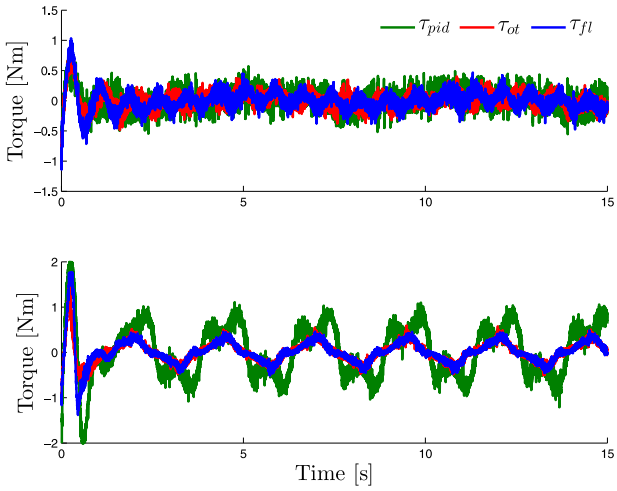


Fig. 6. Time evolution of the applied torque $\tau(t)$ obtained for $\tau_{\text{fl}}$, $\tau_{\text{ot}}$, and $\tau_{\text{pid}}$, with $\omega = 1$ (top) and $\omega = 2.5$ (bottom).

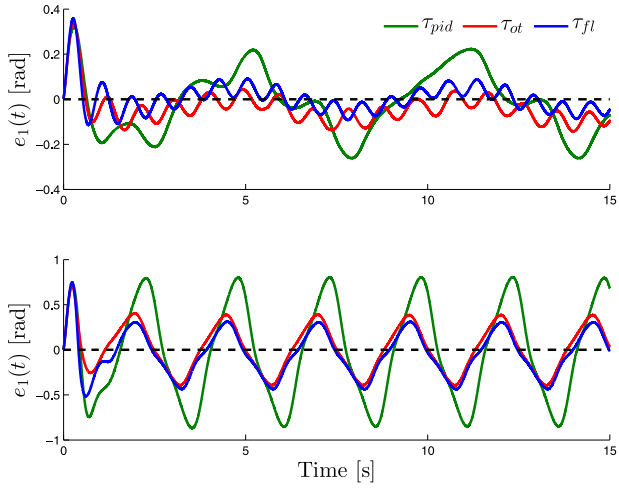


Fig. 7. Time evolution of the tracking error $e_1(t)$ obtained for $\tau_{\text{fl}}$, $\tau_{ot}$, and $\tau_{\text{pid}}$, with $\omega = 1$ (top) and $\omega = 2.5$ (bottom).

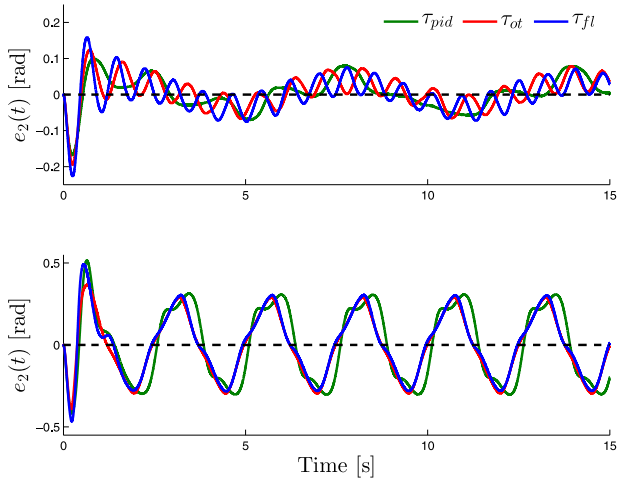


Fig. 8. Time evolution of the regulation error $e_2(t)$ obtained for $\tau_{\text{fl}}$, $\tau_{ot}$, and $\tau_{\text{pid}}$, with $\omega = 1$ (top) and $\omega = 2.5$ (bottom).

with $T = 0.001$ [s] the sampling period and $k$ the integer time index.

### C. Performance Comparison

Now, it is possible proceed to discuss the performance of the controllers presented. With this aim, the tracking error $e_1(t)$ is shown in Fig. 7, where the top plot shows the time evolution of this signal for $\omega = 1$ [rad/s], whereas the bottom plot depicts results for $\omega = 2.5$ [rad/s]. Likewise, the regulation error $e_2(t)$ is depicted in Fig. 8, with $\omega = 1$ [rad/s] for the top plot and $\omega = 2.5$ [rad/s] for the bottom plot.

For a better interpretation of the meaning of the information presented in Figs. 7 and 8, in Table II the mean absolute value (MAV) of the error vector $\boldsymbol{e}(t)$, the RMS value of the error vector $\boldsymbol{e}(t)$, and the RMS value of the applied torque $\tau(t)$ are computed. The MAV index of $\boldsymbol{e}(t)$ is computed as

$$\text{MAV}\{\boldsymbol{e}(t)\} = \frac{1}{t_2 - t_1} \int_{t_1}^{t_2} \left[ |e_1(\rho)| + |e_2(\rho)| \right] d\rho$$

TABLE II
MAV AND RMS INDEXES FOR $t_1 \leq t \leq t_2$

| Index [Units] | $\tau_{\text{pid}}$ | $\tau_{\text{ot}}$ (∗%) | $\tau_{\text{fl}}$ (∗%) |
|---|---|---|---|
| | For $\omega = 1$ [rad/s], $t_1 = 8.71$ [s], and $t_2 = 15$ [s]. | | |
| MAV$\{\boldsymbol{e}(t)\}$ [rad] | 0.1341 | 0.0864 (35.55%) | **0.0656 (51.06%)** |
| RMS$\{\boldsymbol{e}(t)\}$ [rad] | 0.1405 | 0.0772 (45.05%) | **0.0567 (59.65%)** |
| RMS$\{\tau(t)\}$ [N·m] | 0.1360 | **0.1123 (17.44%)** | 0.1151 (15.40%) |
| | For $\omega = 2.5$ [rad/s], $t_1 = 9.97$ [s], and $t_2 = 15$ [s]. | | |
| MAV$\{\boldsymbol{e}(t)\}$ [rad] | 0.6863 | 0.3784 (44.86%) | **0.3626 (47.16%)** |
| RMS$\{\boldsymbol{e}(t)\}$ [rad] | 0.5858 | 0.3116 (46.80%) | **0.3034 (48.21%)** |
| RMS$\{\tau(t)\}$ [N·m] | 0.5163 | 0.3891 (24.64%) | **0.3857 (25.29%)** |

Percentage means the improvement with respect to $\tau_{\text{pid}}$. Best performance in **bold**.

the RMS value of $\boldsymbol{e}(t)$ is given by

$$\text{RMS}\{\boldsymbol{e}(t)\} = \sqrt{\frac{1}{t_2 - t_1}\int_{t_1}^{t_2} \left[|e_1(\rho)|^2 + |e_2(\rho)|^2\right] d\rho}$$

and the RMS value of $\tau(t)$ is

$$\text{RMS}\{\tau(t)\} = \sqrt{\frac{1}{t_2 - t_1}\int_{t_1}^{t_2} |\tau(\rho)|^2 d\rho}.$$

Specifically, Table II shows results for an angular velocity $\omega = 1$ [rad/s], an initial time $t_1 = 8.71$ [s] and a final time $t_2 = 15$ [s], as well as the results for $\omega = 2.5$ [rad/s], $t_1 = 9.97$ [s], and $t_2 = 15$ [s]. The time interval $t_1 \leq t \leq t_2$ is selected with the purpose of eliminating the transitory response and analyzing a complete number of signal periods of the desired trajectory $q_{d1}(t)$ in (57). For $\omega = 1$, one period is analyzed and for $\omega = 2.5$, two periods are analyzed. The percentages of improvement shown in Table II are computed with respect to the numerical index obtained for $\tau_{\text{pid}}$.

As can be seen in Figs. 7 and 8, and Table II, the performance of the nonlinear algorithms $\tau_{\text{fl}}$ and $\tau_{\text{ot}}$ is significantly better compared with the PID controller $\tau_{\text{pid}}$ for both the slow trajectory $q_{d1}(t)$ using $\omega = 1$ and the fast trajectory $q_{d1}(t)$ using $\omega = 2.5$, where the tracking error is improved by up to 50%. Hence, the simplicity of the PID algorithm $\tau_{\text{pid}}$ is paid by introducing large error values.

Comparing the performance of the nonlinear controllers $\tau_{\text{fl}}$ and $\tau_{\text{ot}}$, it is remarkable that, for the tracking of $q_{d1}(t)$ with $\omega = 1$, the proposed controller $\tau_{\text{fl}}$ performs significantly better than the output tracking algorithm $\tau_{\text{ot}}$, where $\tau_{\text{fl}}$ reduces the RMS error by 59.65% with respect to the PID controller $\tau_{\text{pid}}$, while $\tau_{\text{ot}}$ improves the error by 45.05%, this at the cost of a slightly greater control action for $\tau_{\text{fl}}$. However, for $\omega = 2.5$, the proposed algorithm $\tau_{\text{fl}}$ performs better than the output tracking controller $\tau_{\text{ot}}$ even with a smaller control action.

Also note that, for $q_{d1}(t)$ with $\omega = 1$, the values of the applied torque are RMS$\{\tau_{\text{fl}}\} = 0.1151$ [N·m] and RMS$\{\tau_{\text{ot}}\} = 0.1123$ [N·m], which means that the torque applied by the proposed controller $\tau_{\text{fl}}$ is 2.5% bigger. For $q_{d1}(t)$ with $\omega = 2.5$, the RMS values are RMS$\{\tau_{\text{fl}}\} = 0.3857$ [N·m] and RMS$\{\tau_{\text{ot}}\} = 0.3891$ [N·m], which means that the torque applied by the output tracking controller $\tau_{\text{ot}}$ is 0.88% bigger. In both experiments, the 5% tuning criterion of difference of the RMS$\{\tau\}$ of one controller with respect to the other one is satisfied.

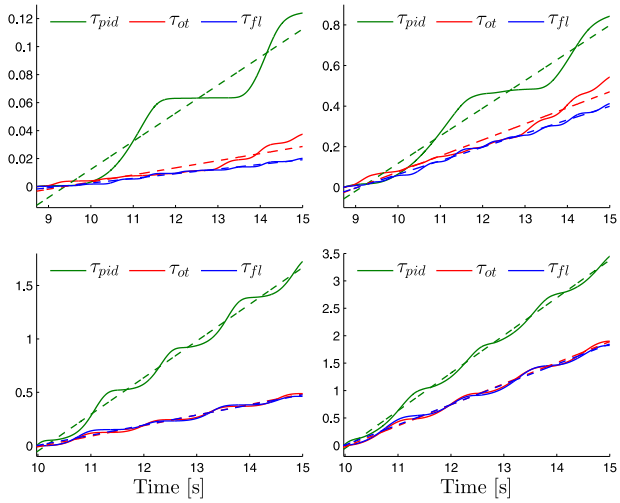


Fig. 9. IAE$(t)$ and ISE$(t)$ indexes obtained for the algorithms in comparison for $t_1 \leq t \leq t_2$. Time evolution of ISE$(t)$ index for $\omega = 1$ (top-left), time evolution of ISE$(t)$ index for $\omega = 2.5$ (bottom-left), time evolution of IAE$(t)$ index for $\omega = 1$ (top-right), and time evolution IAE$(t)$ index for $\omega = 2.5$ (bottom-right). Dashed signals depict the line of best fit for each signal with the same color.

TABLE III
FINAL VALUES AND PARAMETERS OF THE LINE OF BEST FIT $l = mt + b$ FOR BOTH IAE$(t)$ AND ISE$(t)$ INDEXES

| | IAE$(t_2)$ | $m$ | $b$ | ISE$(t_2)$ | $m$ | $b$ |
|---|---|---|---|---|---|---|
| | For $\omega = 1$ [rad/s], $t_1 = 8.71$ [s], and $t_2 = 15$ [s]. | | | | | |
| $\tau_{\text{pid}}$ | 0.8428 | 0.1361 | −1.2436 | 0.1240 | 0.0200 | −0.1881 |
| $\tau_{\text{ot}}$ | 0.5432 | 0.0790 | −0.7140 | 0.0374 | 0.0051 | −0.0476 |
| $\tau_{\text{fl}}$ | **0.4124** | **0.0671** | **−0.6073** | **0.0202** | **0.0033** | **−0.0308** |
| | For $\omega = 2.5$ [rad/s], $t_1 = 9.97$ [s], and $t_2 = 15$ [s]. | | | | | |
| $\tau_{\text{pid}}$ | 3.4493 | 0.6861 | −6.9144 | 1.7250 | 0.3433 | −3.4832 |
| $\tau_{\text{ot}}$ | 1.9017 | 0.3835 | −3.8598 | 0.4881 | 0.0990 | −0.9992 |
| $\tau_{\text{fl}}$ | **1.8223** | **0.3683** | **−3.6749** | **0.4626** | **0.0945** | **−0.9411** |

Best performance in **bold**.

Finally, the integral of absolute error (IAE) and integral of squared error (ISE) indexes computed as a function of time $t \in [t_1, t_2]$ are given by

$$\text{IAE}(t) = \int_{t_1}^{t} \left[|e_1(\rho)| + |e_2(\rho)|\right] d\rho$$

$$\text{ISE}(t) = \int_{t_1}^{t} \left[|e_1(\rho)|^2 + |e_2(\rho)|^2\right] d\rho$$

respectively. Those indexes are depicted in Fig. 9. Specifically, the top-left plot shows ISE$(t)$ for $\omega = 1$, the bottom-left plot shows ISE$(t)$ for $\omega = 2.5$, the top-right plot depicts IAE$(t)$ for $\omega = 1$, and the bottom-right plot shows IAE$(t)$ for $\omega = 2.5$. Table III shows the final values IAE$(t_2)$ and ISE$(t_2)$ for both $\omega = 1.0$ and $\omega = 2.5$. As can be seen in Fig. 9 and Table III, the proposed controller performs the best in every case, presenting

the smallest final values at $t = 15$. Also Fig. 9 shows the line of best fit $l = mt + b$, with $m$ the slope and $b$ the offset, for each plotted signal. The line of best fit can be used as a prediction of the error behavior and was computed using the MATLAB function polyfit, which fits a line to the data in a least squares sense. The characteristics of these lines are shown and compared in Table III, where smaller values of both slope and offset can be interpreted as a better performance. The best performance of the proposed controller is verified.

## VII. Conclusion

A new trajectory tracking controller applied to the Furuta pendulum, where the arm tracks a desired time-varying trajectory, and the pendulum remains regulated at the upward position, was introduced in this paper. The main theoretical result consisted in proving that if the output function converges to zero in an exponential form and the trajectories of the internal dynamics are UUB, then the error state of the overall closed-loop system remains UUB as well. Real-time experiments confirmed the validity of the main result.

About the performance comparison, a PID and an output tracking controller were compared with the new algorithm, which presented the best performance. It is important to highlight that in order to obtain a fair comparison, friction compensation in the output tracking controller in (56) has been added, which is also considered a contribution of this work.

Our present study is focused in the application of the proposed ideas to other underactuated mechanical systems. Other possible extension is the addition of the integral action on the output function $y(t)$ in the proposed control law in (11). The integral action may improve the robustness to disturbances, inducing a second-order system behavior in the time evolution of the output function $y(t)$, which could improve the performance in the tracking of the arm and in the regulation of the pendulum.

## Appendix A

The explicit expression of $\boldsymbol{w}_1$ introduced in (20) is given by

$$\boldsymbol{w}_1(\zeta_1, \boldsymbol{\eta}) = \begin{bmatrix} w_{11} & w_{12} & w_{13} \end{bmatrix}^T \tag{61}$$

where

$$\begin{aligned} w_{11} &= -\frac{\Delta_1\theta_4\eta_1 + \Delta_2\theta_4\eta_2 + \theta_4\eta_3 - \zeta_1\theta_4}{\theta_4 - \theta_3\cos(\eta_2)} \\ w_{12} &= \frac{[\Delta_1\eta_1 + \Delta_2\eta_2 - \zeta_1]\theta_3\cos(\eta_2) + \theta_4\eta_3}{\theta_4 - \theta_3\cos(\eta_2)} \\ w_{13} &= -\frac{\theta_3}{\theta_4}\sin(\eta_2)\dot{\eta}_1\dot{\eta}_2 + \frac{\theta_2}{2\theta_4}\sin(2\eta_2)\dot{\eta}_1^2 \\ &\quad + \frac{\theta_5}{\theta_4}\sin(\eta_2) - \frac{\theta_7}{\theta_4}\dot{\eta}_2. \end{aligned}$$

The expressions of $\dot{\eta}_1$ and $\dot{\eta}_2$ are given in (19).

The explicit expression of $\boldsymbol{w}_2$ introduced in (20) is given by

$$\boldsymbol{w}_2(t, \zeta_1, \boldsymbol{\eta}) = \begin{bmatrix} 0 & 0 & w_{23} \end{bmatrix}^T \tag{62}$$

where

$$w_{23} = \frac{\theta_3}{\theta_4}\cos(\eta_2)\ddot{q}_{d1} + \frac{\theta_2}{2\theta_4}\sin(2\eta_2)\dot{q}_{d1}^2 - \frac{\theta_2}{\theta_4}\sin(2\eta_2)\dot{q}_{d1}\dot{\eta}_1.$$

The linear version of the function $\boldsymbol{w}_1(0, \boldsymbol{\eta})$ around of the origin of $\boldsymbol{\eta}$ is obtained as

$$\dot{\boldsymbol{\eta}} = A\boldsymbol{\eta} \tag{63}$$

where

$$A = \begin{bmatrix} \Delta_1 G_{10} & \Delta_2 G_{10} & G_{10} \\ -\Delta_1 G_{20} & -\Delta_2 G_{20} & -G_{10} \\ \theta_4^{-1}\theta_7\Delta_1 G_{20} & \theta_4^{-1}[\theta_5 + \theta_7\Delta_2 G_{20}] & \theta_4^{-1}\theta_7 G_{10} \end{bmatrix} \tag{64}$$

with

$$G_{10} = \frac{-\theta_4}{\theta_4 - \theta_3},\ G_{20} = \frac{-\theta_3}{\theta_4 - \theta_3}.$$

Note that $A$ in (64) corresponds to the explicit expression of the matrix $A$ defined in (22).

By applying the Routh–Hurwitz criterion, the conditions for $A$ to be Hurwitz are

$$\Delta_2 > \kappa_1 = \frac{\Delta_1 G_{10} + \theta_4^{-1}\theta_7 G_{10}}{G_{20}} \tag{65}$$

and

$$\begin{aligned} \Delta_2 > \kappa_2 = &\frac{G_{10}\theta_7\Delta_1^2 + [\theta_4^{-1}G_{10}\theta_7^2 - G_{10}\theta_5 - \theta_5]\Delta_1}{G_{20}\theta_7\Delta_1 - G_{20}\theta_5} \\ &- \frac{\theta_4^{-1}G_{10}\theta_5\theta_7}{G_{20}\theta_7\Delta_1 - G_{20}\theta_5}. \end{aligned} \tag{66}$$

It is easy to prove that $\kappa_2$ is a dominant condition over $\kappa_1$, i.e.,

$$\kappa_2(\theta_i, \Delta_1) > \kappa_1(\theta_i, \Delta_1)\ \ \forall\Delta_1 \in \mathbb{R}^+. \tag{67}$$

Therefore, if the condition (66) is satisfied, all the roots of the matrix $A$ are in the left-half of the complex plane. Note that the condition in (66) corresponds to the explicit expression of the inequality in (48).

## References


[1] M. W. Spong, *Underactuated Mechanical Systems*. London, U.K.: Springer-Verlag, 1998.

[2] K. Furuta, M. Yamakita, and S. Kobayashi, "Swing up control of inverted pendulum," in *Proc. 1991 Int. Conf. Ind. Electron., Control Instrum.*, Kobe, Japan, Oct. 1991, vol. 3, pp. 2193–2198.

[3] K. Furuta, M. Yamakita, and S. Kobayashi, "Swing-up control of inverted pendulum using pseudo-state feedback," *J. Syst. Control Eng.*, vol. 206 no. 4, pp. 263–269, 1992.

[4] I. Fantoni and R. Lozano, *Non-Linear Control for Underactuated Mechanical Systems*. London, U.K.: Springer-Verlag, 2002.

[5] J. A. Acosta, "Furuta's Pendulum: A conservative nonlinear model for theory and practice," *Math. Problems Eng.*, vol. 2010, pp. 1–29, 2010.

[6] J. Mayr, F. Spanlang, and H. Gattringer, "Mechatronic design of a self-balancing three-dimensional inertia wheel pendulum," *Mechatronics*, to be published.

[7] I. Soto and R. Campa, "Modelling and control of a spherical inverted pendulum on a five-bar mechanism" *Int. J. Adv. Robot. Syst.,"* vol. 12, no. 95, pp. 1–16, 2015.

[8] F. B. Mathis, R. Jafari and R. Mukherjee, "Impulsive actuation in robot manipulators: Experimental verification of pendubot swing-up," *IEEE/ASME Trans. Mechatron.*, vol. 19, no. 4, pp. 1469–1474, Aug. 2014.

[9] M. Zhang and T. Tarn, "Hybrid control of the Pendubot," *IEEE/ASME Trans. Mechatron.*, vol. 7, no. 1, pp. 79–86, Mar. 2002.

[10] R. Ortega, M. W. Spong, F. Gomez-Estern, and G. Blankenstein, "Stabilization of a class of underactuated mechanical systems via interconnection and damping assignment," *IEEE Trans. Autom. Control*, vol. 47, no. 8, pp. 1218–1233, Aug. 2002.

[11] J. Sandoval, R. Kelly, and V. Santibáñez, "Interconnection and damping assignment passivity-based control of a class of underactuated mechanical systems with dynamic friction," *Int. J. Robust Nonlinear Control*, vol. 21, no. 7, pp. 738–751, 2011.
[12] A. P. Singh, F. S. Kazi, N. M. Singh, and P. Srivastava,, "PI$^{\alpha}$ D$^{\beta}$ controller design for underactuated mechanical systems," in *Proc. 12th Int. Conf. Control Autom. Robot. Vis.*, Guangzhou, China, Dec. 2012, pp. 1654–1658.
[13] A. Soria-López, J. C. Martínez-García, and C. F. Aguilar-Ibañez, "Experimental evaluation of regulated non-linear under-actuated mechanical systems via saturation-functions-based bounded control: The cart-pendulum system case," *IET Control Theory Appl.*, vol. 7, no. 12, pp. 1642-1650, 2013.
[14] C. Aguilar-Ibáñez, M. S. Suarez-Castañon, and N. Cruz-Cortés, "Output feedback stabilization of the inverted pendulum system: A Lyapunov approach," *Nonlinear Dynamics*, vol. 70, no. 1, pp. 767–777, 2012.
[15] C. Aguilar-Ibañez, M.S. Suárez-Castañón, and O. Gutiérres-Frias, "The direct Lyapunov method for the stabilisation of the Furuta pendulum," *Int. J. Control*, vol. 83, no. 11, pp. 2285–2293, 2010.
[16] C. Aguilar-Ibáñez and H. Sossa-Azuela, "Stabilization of the Furuta pendulum based on a Lyapunov function," *Nonlinear Dynamics*, vol. 49, no. 1/2, pp. 1–8, 2007.
[17] T. Turker, H. Gorguna, and G. Cansevera, "Stabilisation of a class of 2-DOF underactuated mechanical systems via direct Lyapunov approach," *Int. J. Control*, vol. 86, no. 6, pp. 1137–1148, 2013.
[18] D. E. Chang, "Pseudo-energy shaping for the stabilization of a class of second-order systems," *Int. J. Robust Nonlinear Control*, vol. 2, no. 18, pp. 1999–2013, 2012.
[19] D. E. Chang, "Stabilizability of controlled lagrangian systems of two degrees of freedom and one degree of under-actuation by the energy-shaping method," *IEEE Trans. Autom. Control*, vol. 55, no. 8, pp. 1888–1893, Aug. 2010.
[20] G. Pujol and L. Acho, "Stabilization of the Furuta Pendulum with backlash using $H_{\infty}$-LMI technique: Experimental validation," *Asian J. Control*, vol. 12, no. 4, pp. 460–467, 2010.
[21] M.-S. Park and D. Chwa, "Swing-up and stabilization control of inverted-pendulum systems via coupled sliding-mode control method," *IEEE Trans. Ind. Electron.*, vol. 56, no. 9, pp. 3541–3555, Sep. 2009.
[22] I. Hassanzadeh, S. Mobayen, and A. Harifi, "Input-output feedback linearization cascade controller using genetic algorithm for rotary inverted pendulum system," *Amer. J. Appl. Sci.*, vol. 5, no. 10, pp. 1322–1328, 2008.
[23] J. A. Acosta and M. López-Martínez, "Constructive feedback linearization of underactuated mechanical systems with 2-DOF," in *Proc. 44th IEEE Conf. Decision Control*, Seville, Spain, Dec. 2005, pp. 4909–4914.
[24] V. Nath, R. Singh, and K. Gupta, "Natural frequency based swing up of rotary inverted pendulum and its stabilization," *Int. J. Sci. Res. Eng. Technol.*, vol. 3, no. 3, pp. 655–658, 2014.
[25] J. Aracil, J. A. Acosta, and F. Gordillo, "A nonlinear hybrid controller for swinging-up and stabilizing the Furuta pendulum," *Control Eng. Practice*, vol. 21, no. 8, pp. 989–993, 2013.
[26] P. Seman, B. Rohal'-Ilkiv, M. Juh'as, and M. Salaj, "Swinging up the Furuta pendulum and its stabilization via model predictive control," *J. Electr. Eng.*, vol. 64, no. 3, pp. 152–158, 2013.
[27] M. Izutsu, Y. Pan, and K. Furuta, "Swing-up of Furuta pendulum by nonlinear sliding mode control," *SICE J. Control, Meas. Syst. Integr.*, vol. 1, no. 1, pp. 12–17, 2011.
[28] P. X. La Hera, L. B. Freidovich, A. S. Shiriaev, and U. Mettin, "New approach for swinging up the Furuta pendulum: Theory and experiments," *Mechatronics*, vol. 19, no. 8, pp. 1240–1250, 2009.
[29] F. Gordillo, J. A. Acosta, and J. Aracil, "A new swing-up law for the Furuta pendulum," *Int. J. Control*, vol. 76, no. 8, pp. 836–844, 2003.
[30] M. Azad and R. Featherstone, "Angular momentum based balance controller for an under-actuated planar robot," *Auton. Robots*, to be published.
[31] M. N. Huda and Hongnian Yu, "Trajectory tracking control of an under-actuated capsubot," *Auton. Robot.*, vol. 39, no. 2, pp. 183–198, 2015.
[32] S. Rudra, R. K. Barai, and M. Maitra, "Nonlinear state feedback controller design for underactuated mechanical system: A modified block backstepping approach," *ISA Trans.*, vol. 53, no. 2, pp. 317–326, 2014.
[33] Y. Liu, H. Yu, S. Wan, and T. Yang, "On tracking control of a pendulum-driven cart-pole underactuated system," *Int. J. Model., Identification Control*, vol. 4, no. 4, pp. 357–372, 2008.
[34] H. Yu, Y. Liu, and T. Yang, "Closed-loop tracking control of a pendulum-driven cart-pole underactuated system," *J. Syst. Control Eng.*, vol. 222, no. 2, pp. 109–125, 2008.
[35] M. I. El-Hawwary, A. L. Elshafei, H. M. Emara, and H. A. A. Fattah, "Adaptive fuzzy control of the inverted pendulum problem," *IEEE Trans. Control Syst. Technol.*, vol. 14, no. 6, pp. 1135–1144, Nov. 2006.
[36] F. Mazenc and S. Bowong, "Tracking trajectories of the cart-pendulum system," *Automatica*, vol. 39, no. 4, pp. 677–684, 2003.
[37] M. D. Berkemeier and R.S. Fearing, "Tracking fast inverted trajectories of the underactuated Acrobot," *IEEE Trans. Robot. Autom.*, vol. 15, no. 4, pp. 740–750, Aug. 1999.
[38] W. N. White, J. Patenaude, M. Foss, and D. García, "Direct Lyapunov approach for tracking control of underactuated mechanical systems," in *Proc. 2009 Amer. Control Conf.*, St. Louis, MO, USA, Jun. 2009, pp. 1341–1346.
[39] M. Ramírez-Neria, H. Sira-Ramírez, R. Garrido-Moctezuma, and A. Luviano-Juárez, "Linear active disturbance rejection control of underactuated systems: The case of the Furuta pendulum," *ISA Trans.*, vol. 53, no. 4, pp. 920–928, 2014.
[40] C. Aguilar-Ibáñez and H. Sira-Ramírez, "A linear differential flatness approach to controlling the Furuta pendulum," *IMA J. Math. Control Inform.*, vol. 24, no. 1, pp. 31–35, 2007.
[41] Q. Yan, "Output tracking of underactuated rotary inverted pendulum by nonlinear controller," in *Proc. 42nd IEEE Conf. Decision Control*, Maui, Hawaii, Dec. 2003, vol. 3, pp. 2395–2400.
[42] T. C. Kuo, Y. J. Huang, and B. W. Hong, "Adaptive PID with sliding mode control for the rotary inverted pendulum system," in *Proc. IEEE/ASME Int. Conf. Adv. Intell. Mechatron.*, Singapore, Jul. 2009, pp. 1804–1809.
[43] H. K. Khalil, *Nonlinear Systems*. Upper Saddle River, NJ, USA: Prentice-Hall, 2002.
[44] J.-J. E. Slotine and W. Li, . Englewood Cliffs, NJ, USA: Prentice Hall, 1991.
[45] L. Sciavicco and B. Siciliano, *Modelling and Control of Robot Manipulators*. London, U.K.: Springer-Verlag, 2000.
[46] B. S. Cazzolato and Z. Prime, "On the dynamics of the Furuta pendulum," *J. Control Sci. Eng.*, vol. 2011, pp. 1–8, 2011.
[47] R. Kelly, V. Santibáñez, and A. Loría, *Control of Robot Manipulators in Joint Space*. London, U.K.: Springer-Verlag, 2005.
[48] R. C. Dorf and R. H. Bishop, *Modern Control Systems*. Englewood Cliffs, NJ, USA: Prentice-Hall, 2011.
[49] "Video 1: Slow trajectory." Internet: https://youtu.be/pdXGf2kfEfU, Feb. 14, 2014 [Oct. 10, 2015].
[50] "Video 2: Fast trajectory." Internet: https://youtu.be/yUKxUthV3po, Feb. 14, 2014 [Oct. 10, 2015].

**Carlos Aguilar-Avelar** received the B.Sc. degree in electronics engineering with specialization in digital systems from the Instituto Tecnológico de Los Mochis, Los Mochis, Mexico, in 2011, and the M.Sc. degree in digital systems with specialization in control systems from the Instituto Politécnico Nacional-CITEDI, Tijuana, Mexico, in 2013, where he is currently working toward the Ph.D. degree in digital systems at the Laboratory of Systems and Control.

His research interests include the analysis and control of underactuated mechatronic systems, nonlinear control, adaptive control, and neural network-based control.

**Javier Moreno-Valenzuela** (M'15) received the B.Sc. degree in electronics engineering from the Instituto Tecnológico de Culiacán, Sinaloa, Mexico, in 1997, and the Ph.D. degree in automatic control from Ensenada Center for Scientific Research and Higher Education, Ensenada, Mexico, in 2002.

From 2004 to 2005, he was a Postdoctoral Fellow with the Université de Liège, Liège, Belgium. He is currently with the Instituto Politécnico Nacional-CITEDI, Tijuana, Mexico. He is the author of more than 40 journal papers. His research interests include nonlinear systems, complex systems, mechatronics and intelligent systems.

Dr. Moreno-Valenzuela was a Reviewer of a number of prestigious scientific journals. He was an Invited Editor of *International Journal of Advanced Robotic Systems* and *Mathematical Problems in Engineering.*